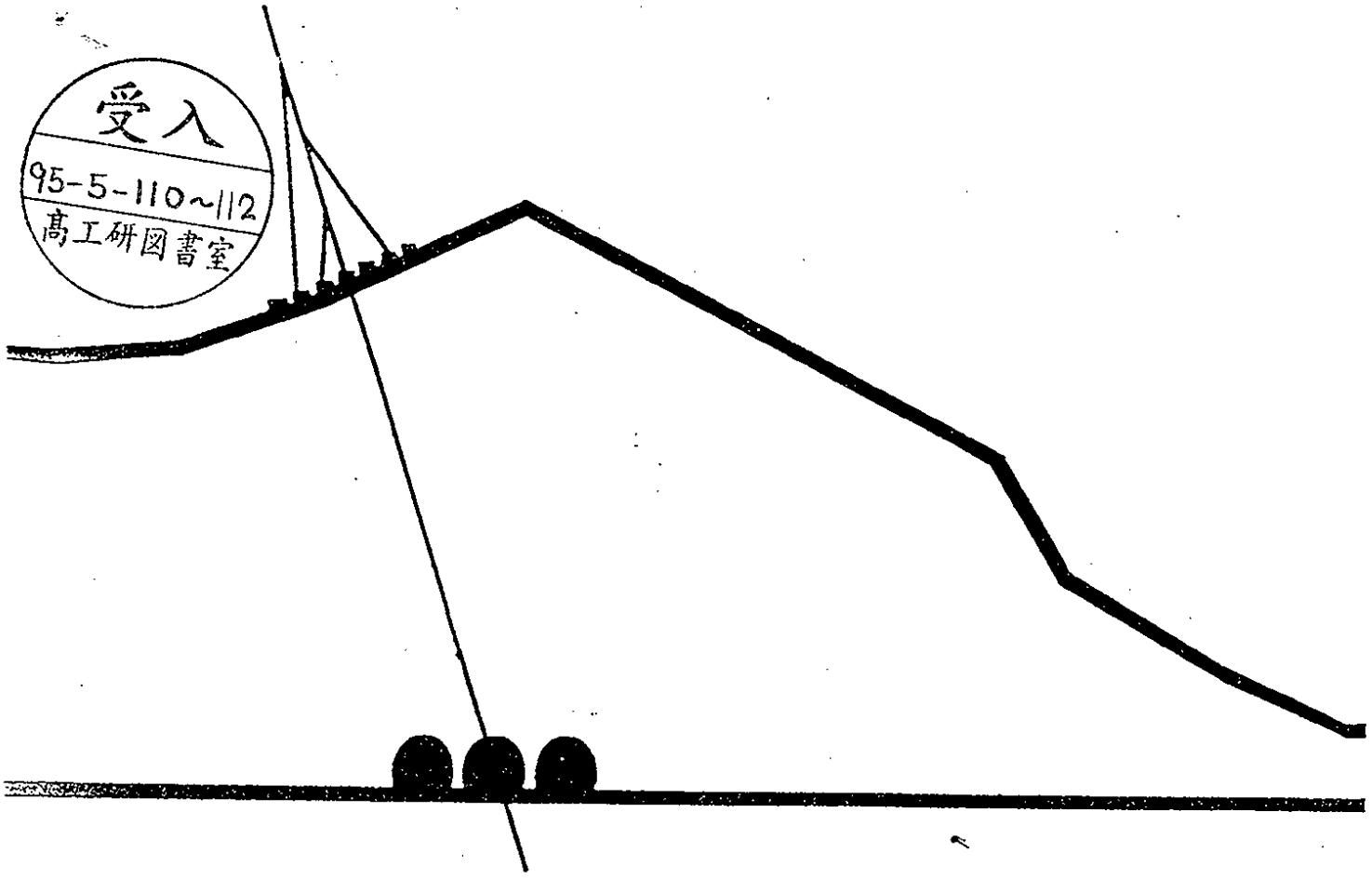

Underground Muon Physics at MACRO

LNGS - 94/114
December 1994

Search for Magnetic Monopoles with the MACRO Track-etch Detector

LNGS - 94/115
December 1994

A Search for Cosmic Point Sources of Muons and for Seasonal Variations in the Underground Muon Flux with the MACRO Detector

LNGS - 94/116
December 1994

(MACRO Collaboration)

INFN - Laboratori Nazionali del Gran Sasso

LNGS - 94/114
December 1994

MACRO/PUB 94/1

Underground Muon Physics at MACRO

S. Ahlen[3], M. Ambrosio[12], R. Antolini[7], G. Auriemma[14,a], R. Baker[11], A. Baldini[13], G.C. Barbarino[12], B.C. Barish[4], G. Battistoni[6,19*], R. Bellotti[1], C. Bemporad[13], P. Bernardini[10], H. Bilokon[6], V. Bisi[16], C. Bloise[6], C. Bower[8], S. Bussino[14], F. Cafagna[1], M. Calicchio[1], D. Campana[12], M. Carboni[6], S. Cecchini[2,b], F. Cei[13], V. Chiarella[6], R. Cormack[3], A. Corona[14], S. Coutu[11], G. De Cataldo[1], H. Dekhissi[2,c], C. De Marzo[1], I. De Mitri[9], M. De Vincenzi[14,d], A. Di Credico[7], E. Diehl[11], O. Erriquez[1], C. Favuzzi[1], C. Forti[6], P. Fusco[1], G. Giacomelli[2], G. Giannini[13,e], N. Giglietto[1], M. Goretti[14], M. Grassi[13], P. Green[15,18*], A. Grillo[6], F. Guarino[12], P. Guarnaccia[1], C. Gustavino[7], A. Habig[8], K. Hanson[11], R. Heinz[8], J.T. Hong[3], E. Iarocci[6,f], E. Katsavounidis[4], E. Kearns[3], S. Kyriazopoulou[4], E. Lamanna[14], C. Lane[5], D. S. Levin[11], P. Lipari[14], G. Liu[4], R. Liu[4], M.J. Longo[11], Y. Lu[15], G. Ludlam[3], G. Mancarella[10], G. Mandrioli[2], A. Margiotta-Neri[2], A. Marin[3], A. Marini[6], D. Martello[10,17*], A. Marzari Chiesa[16], P. Matteuzzi[2], M.N. Mazziotta[1], D.G. Michael[4], S. Mikheyev[7,g], L. Miller[8], M. Mittelbrun[5], P. Monacelli[9], T. Montaruli[1], M. Monteno[16], S. Mufson[8], J. Musser[8], D. Nicoló[13], R. Nolty[4], C. Okada[3], G. Osteria[12], O. Palamara[10], S. Parlati[4,7*], V. Patera[6,f], L. Patrizii[2], B. Pavesi[2], R. Pazzi[13], C.W. Peck[4], J. Petrakis[8,17*], S. Petrera[10], N.D. Pignatano[4], P. Pistilli[10], A. Rainó[1], J. Reynoldson[7], F. Ronga[6], G. Sanzani[2], A. Sanzgiri[15], F. Sartogo[14], C. Satriano[14,a], L. Satta[6,f], E. Scapparone[2], K. Scholberg[4], A. Sciubba[6,f], P. Serra Lugaresi[2], M. Severi[14], M. Sitta[16], P. Spinelli[1], M. Spinetti[6], M. Spurio[2], R. Steinberg[5], J.L. Stone[3], L.R. Sulak[3], A. Surdo[10], G. Tarlé[11], V. Togo[2], V. Valente[6], C.W. Walter[4], R. Webb[15] and W. Worstell[3].

(MACRO Collaboration)

1. Dipartimento di Fisica dell'Università di Bari and INFN, Bari, 70126, Italy
2. Dipartimento di Fisica dell'Università di Bologna and INFN, Bologna, 40126, Italy
3. Physics Department, Boston University, Boston, MA 02215, USA
4. California Institute of Technology, Pasadena, CA 91125, USA
5. Department of Physics, Drexel University, Philadelphia, PA 19104, USA
6. Laboratori Nazionali di Frascati dell'INFN, Frascati (Roma), 00044, Italy
7. Laboratori Nazionali del Gran Sasso dell'INFN, Assergi (L'Aquila), 67010, Italy
8. Depts. of Physics and of Astronomy, Indiana University, Bloomington, IN 47405, USA
9. Dipartimento di Fisica dell'Università dell'Aquila and INFN, L'Aquila, 67100, Italy
10. Dipartimento di Fisica dell'Università di Lecce and INFN, Lecce, 73100, Italy
11. Department of Physics, University of Michigan, Ann Arbor, MI 48109, USA

12. Dipartimento di Fisica dell'Università di Napoli and INFN, Napoli, 80125, Italy
13. Dipartimento di Fisica dell'Università di Pisa and INFN, Pisa, 56010, Italy
14. Dipartimento di Fisica dell'Università di Roma and INFN, Roma, 00185, Italy
15. Physics Department, Texas A&M University, College Station, TX 77843, USA
16. Dipartimento di Fisica Sperimentale dell'Università di Torino and INFN, Torino, 10125, Italy
17. Bartol Research Institute, University of Delaware, Newark, DE 19716, USA
18. Sandia National Laboratory, Albuquerque, NM 87185, USA
19. INFN Sezione di Milano, 20133, Italy
⋆ Current address
a Also Università della Basilicata, Potenza, 85100, Italy
b Also Istituto TESRE/CNR, Bologna, Italy
c Also at Faculty of Science, University Mohamed I, Oujda, Morocco
d Also at Università di Camerino, Camerino, Italy
e Also Università di Trieste and INFN, Trieste, 34100, Italy
f Also Dipartimento di Energetica, Università di Roma, Roma, 00185, Italy
g Also at Institute for Nuclear Research, Russian Academy of Science, Moscow, Russia

Abstract

Recent MACRO studies of underground muon data have produced preliminary results for flux and overburden studies, ultra high energy cosmic ray composition analysis, investigations into the lateral and angular distribution of underground muon tracks within multiple muon bundles, and searches for heavy particles via their delayed muon arrival signature. These studies are also relevant to our understanding and Monte Carlo modelling of cosmic ray shower development.

1 Introduction

Underground muon events at MACRO open many windows on the physical world. One of the most established efforts is the study of cosmic ray composition in the interesting "knee" region of the primary spectrum via underground muon multiplicity distributions. In addition, the large size and excellent tracking ability of the MACRO detector also make possible studies of the muon lateral distribution, which at MACRO can be extended by nearly an order of magnitude in separation over what was possible with previous underground experiments. Additional MACRO analyses address other interesting topics which can be effectively probed by a powerful deep underground detector, including the surface muon flux, lateral and angular muon track separation, and searches for delayed muons, a signature of heavy particle creation in energetic cosmic ray cascades. In addition to their intrinsic interest, these analyses are also relevant to our knowledge of cosmic ray showers themselves, and these efforts continue to improve our modelling and understanding of the fundamental processes which govern cosmic ray cascade development.

The newly completed MACRO detector accumulates underground muon data at the rate of $\simeq 6.6 \times 10^6$ events/live year, of which $\simeq 4.0 \times 10^5$ exhibit multiple muon tracks and $\simeq 1.6 \times 10^3$ are of multiplicity ten or more. Combined with our ever improving ability to model cosmic ray showers, these data represent a unique opportunity to expand our understanding of cosmic ray physics.

2 Vertical Muon Intensity

The vertical muon intensity analysis discussed here is based on data collected with the full lower MACRO detector (72 m×12 m×6 m) over about 500 days starting in July 1991. The aims are the determination of the vertical muon intensity as a function of depth and the study of the muon flux at the surface. Total statistics are about three million muons, an order of magnitude larger than previous published results [1]. The intensity vs. depth relation is determined in solid angle bins defined by their average zenith and azimuthal angles, with slant depth h taken from a military topographical map of the mountain. The entire data sample (single and multiple muons) is used to determine the bin-by-bin vertical muon intensity via:

$$I_\mu(h,\theta,\phi) = \left(\frac{1}{\Delta T \Delta\Omega}\right) \frac{\Sigma_i N_i m_i}{\Sigma_j A_j \epsilon_j / \cos\theta_j}, \tag{1}$$

where ΔT is the live time, N_i is the number of observed events of muon multiplicity m_i in the bin of slant depth h, A_j is the geometric detector acceptance for that bin, ϵ_j is the combined trigger and reconstruction efficiency, and θ_j is the muon zenith angle. The acceptance $A(\theta,\phi)_j$ was calculated using the detailed GMACRO Monte Carlo simulation code based on GEANT [2].

For each solid angle bin the Gran Sasso rock thickness (m) was converted to standard rock slant depth (hg/cm^2) using the average density $\rho = 2.71$ g/cm^3 and the conversion formula estimated in [3]. The solid angle bins were then divided into fifty-four bins of equal slant depth h and width $\Delta h = 100$ hg/cm^2 up to $h = 4800$ hg/cm^2, $\Delta h = 200$ hg/cm^2 thereafter. The MACRO vertical muon intensity as a function of the slant depth h is shown in Fig. 1 for the zenith range $0-60°$. The Frejùs and Nusex results [4] are included for comparison.

In the range $3200-7000$ hg/cm^2 the data are well fitted by the empirical formula

$$I(h) = A \left(\frac{h_0}{h}\right)^{\alpha} e^{-h/h_0}, \tag{2}$$

where $A = (1.97 \pm 0.02) \times 10^{-6}$ cm^{-2}s^{-1}sr^{-1}, $\alpha = 1.15 \pm 0.01$, and $h_0 = 983 \pm 2$ hg/cm^2. For this fit χ^2/DoF=1.8. Using the Frejùs function

$$I(h) = B(h_1/h)^2 e^{-h/h_1} \tag{3}$$

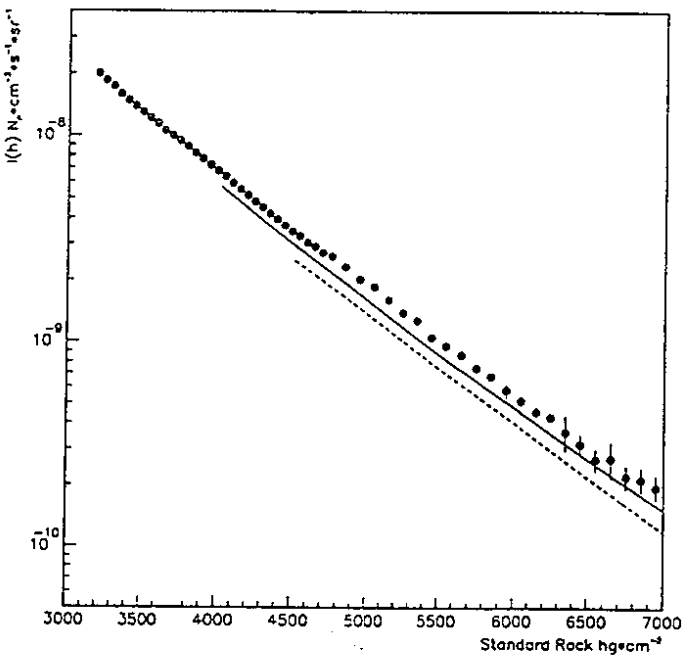

Figure 1: Vertical muon intensity as a function of standard rock slant depth. The crosses represent MACRO data. The solid and dashed lines correspond to the Frejùs and Nusex results, respectively.

in the same range we obtain $B = (1.77 \pm 0.03) \times 10^{-6}$ cm^{-2}s^{-1}sr^{-1} and $h_1 = 1237 \pm 4$ hg/cm^2. with χ^2/DoF=2.4. The quoted errors take into account the statistical uncertainties and the Gran Sasso map resolution of ~ 10 m.

The difference between the Frejùs curve and the MACRO data corresponds to one standard deviation in the Frejùs fitted parameters. Assuming for the surface muon flux the $\cos\theta$ dependence given in [5]:

$$\Phi(E_\mu, \theta) = A \, \frac{E_\mu^{-\gamma}}{\cos\theta}, \tag{4}$$

where Φ is in cm^{-2}s^{-1}sr^{-1}TeV^{-1} and E_μ is in TeV, we used a minimum χ^2 method to unfold the muon flux from the experimental intensity, through:

$$I_\mu(h.\theta) = \int_0^\infty P(E_\mu, h)\, \Phi(E_\mu, \theta)\, dE_\mu. \tag{5}$$

Here $I_\mu(h,\theta)$ is the experimental intensity integrated over ϕ at constant h and θ, and $P(E_\mu,h)$ is the probability that a muon of energy E_μ survives to depth h. This probability was calculated for the 1-100 TeV energy range relevant to the MACRO detector using a GEANT code especially tuned to the Gran Sasso rock, which includes a detailed description of muon propagation underground and takes fluctuations in energy loss into account. The fit parameters are $A = (1.47 \pm 0.05) \times 10^{-7}$ and $\gamma = 3.70 \pm 0.03$ with $\chi^2/\mathrm{DoF} = 1.1$. We explored the systematic effect of uncertainties in the rock density by varying ρ: an uncertainty of $\frac{\Delta\rho}{\rho} = 1\%$ produces a variation of the order of 3.5% in A and 1% in γ.

Because there are uncertainties in the bremsstrahlung and photonuclear cross sections, the results obtained here depend upon the hard muon energy loss cross sections used by GEANT [2]. We used different sets of survival probabilities to test the sensitivity of the fitted parameters to these uncertainties. For [6], where a different photoproduction cross section [7] is employed, we obtain a variation of $\simeq 2\%$ in both A and γ, but with $\chi^2/\mathrm{DoF} = 2.9$. The overall systematic errors resulting from rock density (for which we assume an uncertainty of $\sim 1\%$) and hard energy loss cross sections may be quoted as $\sim 5\%$ in A and $\sim 3\%$ in γ.

3 Cosmic Ray Composition

This MACRO cosmic ray composition analysis is based on muons collected with all six lower supermodules. We selected "good" runs by requiring uniform streamer tube operating conditions in each supermodule, rendering unbiased track reconstruction independent of muon location. Further event selection was performed using criteria established in previous analyses, described in detail in [8]. The analyzed event sample corresponds to 3295 hr total live time and $\simeq 2.5 \times 10^6$ muon events, of which $\simeq 150,000$ exhibit multiple muon tracks.

Detector effects (inefficiencies, failures of the tracking algorithm, and track shadowing at low separations) prevent us from obtaining an unbiased multiplicity distribution directly from the reconstructed multiplicities on the two projected (wire and strip) views. Furthermore, high multiplicity events can be lost because the tracking algorithm is increasingly inefficient for multiplicities on the order of 8-10. In our previous analysis [8] a considerable

amount of visual scanning was performed in order to account for these effects, but in the present analysis we correct the reconstructed multiplicity using an improved version of the MACRO detector simulation program, based on the GEANT [2] code. This simulation, which includes a detailed description of all the known physics and detector effects (electromagnetic showering down to 500 keV, charge induction of the streamer signal onto the strips, electronic noise, *etc.*), reproduces the experimental data at a satisfactory level of accuracy. These simulated data are used to calculate the correction factors that allow transformation of the number of reconstructed tracks in the two views to an actual muon multiplicity. In this way we assign the multiplicity to each event on an objective basis, reducing considerably the errors in the previous analysis which were dominated by scanning uncertainties.

Fig. 2 shows the multimuon rates for the one, two, and six supermodule event samples. The increase of acceptance with detector size is reflected in the increase in muon rates and sampling of very high multiplicity events. The full-sized MACRO detector collects $\simeq 6.6 \times 10^6$ muon events per year, of which $\simeq 4.0 \times 10^5$ /yr have $N_\mu \geq 2$ and $\simeq 1.6 \times 10^3$/yr have $N_\mu \geq 10$. This allows excellent statistical accuracy on a very wide range of the primary energy spectrum.

We simulated events using two different shower simulation codes: HEMAS [9] with nuclear fragmentation based on the semi-superposition model [10], and SIBYLL [11]. This model is more physically motivated than the HEMAS simulation, being based on the dual parton model [12] with the inclusion of hard processes such as mini-jet production [13]. The multiplicity distributions calculated with the two models have similar behaviors, with single muon rates slightly higher in SIBYLL and multiple muon rates slightly higher in HEMAS. The inclusive muon flux calculated with SIBYLL is about 6% higher than that calculated with HEMAS.

In the present analysis we considered three different primary composition models: light and heavy compositions [14], and a constant mass composition (CMC) with fixed spectral indices [15]. The light and heavy compositions are extreme models: at increasingly higher energies the light composition contains a large proton component while the heavy composition contains a large Fe component. Moreover, the models are constrained to reproduce the known abundances and spectra directly measured at ≤ 100 TeV and to agree with extensive air shower measurements at higher energies. Therefore a comparison of the muon experimental rates with the predictions of these

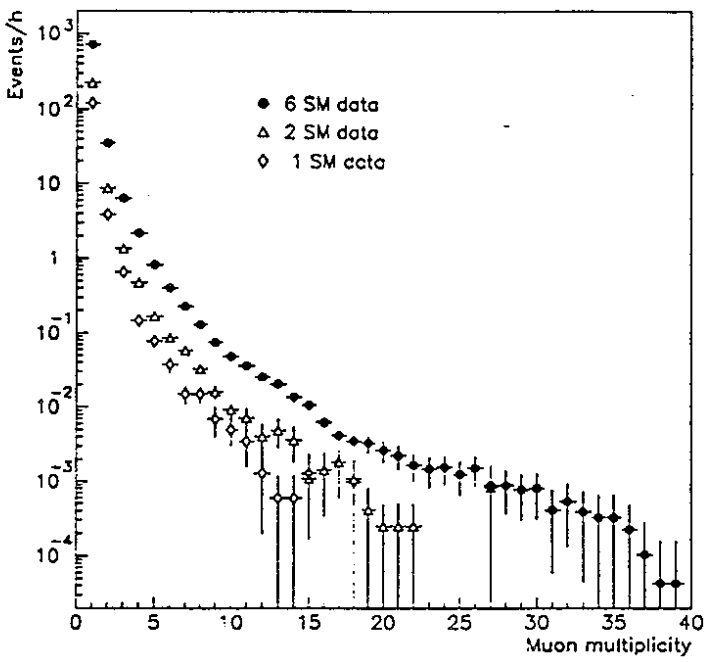

Figure 2: Muon multiplicity distributions for the one, two, and six supermodule data.

models gives an indication of the sensitivity of the experiment to primary composition.

MACRO multimuon events are produced by primaries in the energy range of ~ 50 to $\sim 10^5$ TeV. The range of energy corresponding to the detection of muon events of a particular multiplicity increases as a function of that multiplicity. Specifically, events with detected multiplicities of $N_\mu \leq 4$ originate in interactions of primaries with energies less than a few hundred TeV, while events with $N_\mu \geq 10$ come from primaries in an energy region entirely above the "knee." These results are roughly independent of the primary composition model.

Fig. 3 shows the dependence of the average primary mass $\langle A \rangle$ on energy for the three composition models described above, as well as for the SIGMA model which is based on fits to direct measurements from 1-100 TeV and extrapolated up to the "knee" region [16]. Therefore the SIGMA model can be viewed as a reference $\langle A \rangle$, following the energy dependence of direct measurements at low energy. As one can see from this figure the light and CMC

models are in the same range of $\langle A \rangle$ as the direct measurements. The heavy model, on the other hand, has a completely different energy dependence in nearly the entire energy range relevant to MACRO multimuon events.

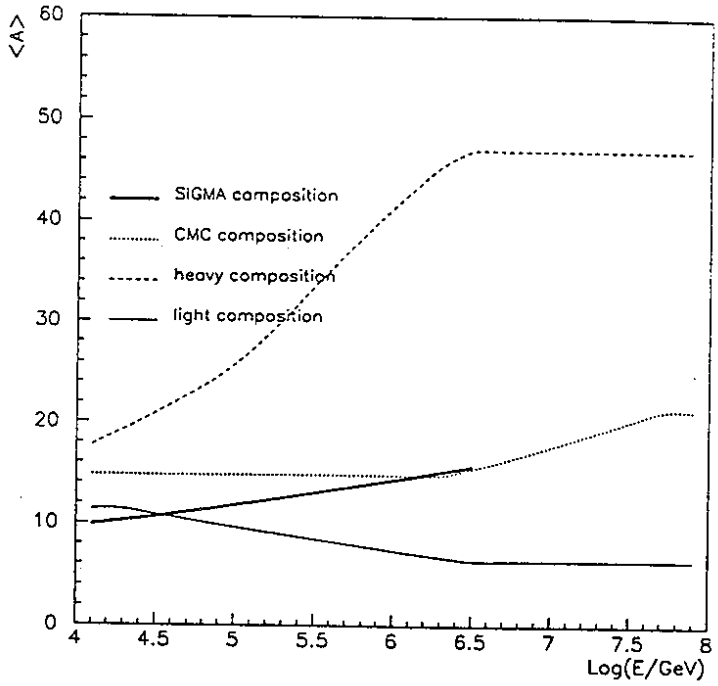

Figure 3: Average primary mass as a function of energy for various composition models.

The ratios between the rates predicted by our Monte Carlo simulation (using HEMAS) and the six supermodule experimental data are shown in Fig. 4. One feature of this figure is that the measured multimuon rates at low multiplicities ($N_\mu \leq 4$) are higher than those predicted by the Monte Carlo regardless of composition model. These events originate in primaries with energies less than a few hundred TeV, for which the three models are very similar and in agreement with direct measurements. We investigated the effects of our present uncertaintites in the rock overburden and muon propagation as possible sources of this disagreement, and found from Monte Carlo simulations that while these uncertainties affect the absolute muon rates they do not affect the shape of the multiplicity distribution.

Fig. 4 shows that our data are inconsistent with the predictions of the

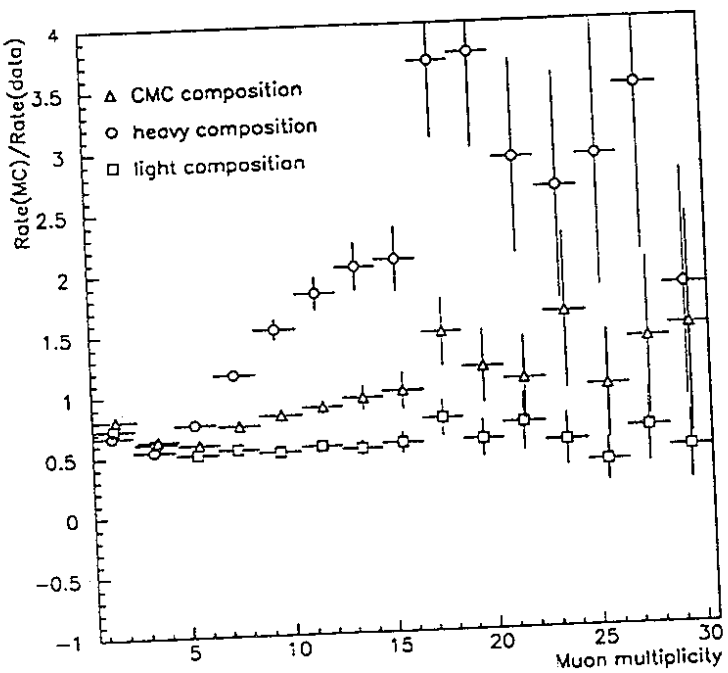

Figure 4: Ratio of predicted to observed event rates for the light, heavy, and constant mass (CMC) compositions.

heavy composition at high multiplicity and favor a lighter model. Therefore we can exclude a primary composition that becomes heavier with increasing energy as dramatically as does the heavy model. The data provide a better fit to models with flat or slowly increasing $\langle A \rangle$ as a function of primary energy, as with the light and CMC models.

4 Muon Decoherence

The lateral distribution of underground muon pairs has been demonstrated to be sensitive to hadronic interaction models, allowing the rejection of some simplified cascade treatments [17]. The analysis of muon pairs collected by the full lower six MACRO supermodules is reported here, extending discussion of the decoherence function up to 70 m, as compared to the previous analysis using only only two supermodules with maximum separation $\simeq$ 20 m.

The previous work used the parametrized results of the HEMAS code [9]

to generate cosmic ray showers, and demonstrated good agreement with Monte Carlo expectations over the entire observable range. But while the parametrized formulae, which give the number and the spatial distribution of the underground muons as function of primary mass, energy, and direction, allowed Monte Carlo analysis to conserve computer time, use of the parametrization ignores the correlation between muon multiplicity and lateral distribution. Therefore we have chosen in this new analysis to perform full simulations of the atmospheric cascade and muon propagation, and discuss a series of improvements in the Monte Carlo procedure below.

The data sample corresponds to about 7600 hr of live time, during which the whole lower part of the MACRO detector [18] was operational, with acceptance of 3100 m^2 sr including the angular distribution of downgoing muons. During this time about 5.8×10^6 muons and 1.9×10^5 muon pairs were reconstructed. The data selection criteria are reported in [19].

In preparing the full HEMAS based Monte Carlo, we investigated several possible systematic effects on the simulation, including:

1. Biases due to the failure of the parametrization to account for the correlation between muon multiplicity and lateral distribution,
2. Uncertainties in the primary interaction cross section,
3. Different possible models of nucleus-nucleus interactions (superposition vs. fragmentation),
4. The treatment of energy loss and multiple scattering in the rock, and
5. The effect of the geomagnetic field on cascade development.

The results generally showed that the dependence of the underground muon separation on the details of the Monte Carlo was weak. A comparison of the full HEMAS based Monte Carlo to the parametrized version using the intermediate constant mass composition [15], for instance, showed that the average muon pair separation increases by only 2% in the more complete version. An increase in the primary interaction cross section raises the height of first interaction, thus causing an increase in the average underground muon separation, but the hadronic mean free path of around 70 g/cm^2 determines that the relative change in height of interaction is only one third the relative change in primary cross section: that is, increasing the primary cross section

by 10% produces only a 3% increase in muon production height. A greater degree of uncertainty affects the nucleus-nucleus interaction model, due to the lack of experimental data for the energies of interest. The HEMAS code handles cascades generated by heavy nuclei (mass A, total energy E) in the superposition scheme, as A independent nucleons of energy E/A. Replacing this with a more realistic model [10] causes larger fluctuations than are expected according to the superposition model, but the decoherence distribution is not affected within the present statistics of the simulated data. Muon transport through the rock was compared to that implemented in GEANT, a more recent simulation developed to model high energy accelerator events [2]. Again, we found no noticeable difference as far as the lateral spread of muons is concerned. Finally, an increase in the average muon separation of about 5% is achieved by considering the affect of the geomagnetic field on shower development.

In Fig. 5 the experimental pair separation distribution for the entire data sample is compared with Monte Carlo predictions for two extreme (light and heavy) composition models [20]. Simulated data are relative to an integrated acceptance of 8.46×10^{10} m^2 s sr., *i. e.* approximately 1000 days for 10^4 m^2 horizontal surface area.

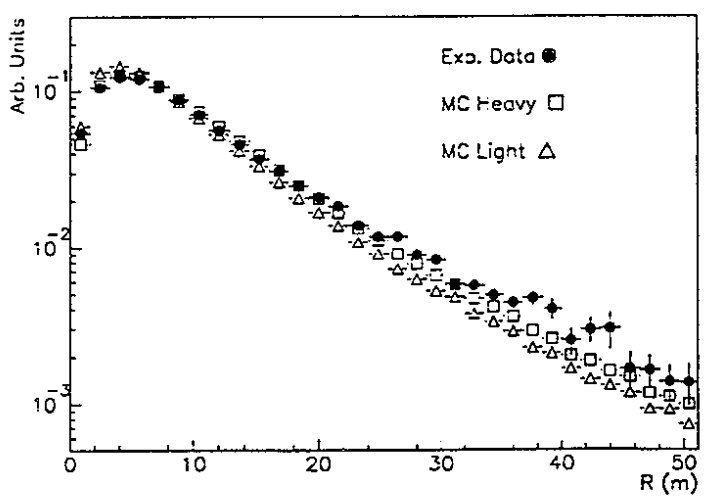

Figure 5: The muon pair separation distribution. The simulated data are relative to an acceptance of 8.46×10^{10} m^2 s sr.

Analysis of the lateral distribution of muon pairs collected with all six

Table 1: *Comparison of Experimental Average Separation in Muon Pairs vs MC Results for Different Zenith Angle Intervals ($h = 3750 \div 4150$ mwe).*

Cos(θ)	R_0 $< D >$ exp. (m)	r.m.s. stat. R_0 $< D >$	Syst. err. $< D >$	MC Light R_0 $< D >$	MC Heavy R_0 $< D >$
$0.5 \div 0.6$	6.50 14.8	0.10 0.2	0.4	5.70 13.3	6.70 14.8
$0.6 \div 0.7$	5.29 13.4	0.05 0.1	0.5	4.53 11.1	5.35 12.3
$0.7 \div 0.8$	4.52 12.5	0.04 0.1	0.7	3.89 9.2	4.53 10.3
$0.8 \div 0.9$	3.91 9.7	0.05 0.1	0.3	3.37 8.1	3.82 8.9
$0.9 \div 1.0$	3.43 7.7	0.04 0.1	0.2	2.99 7.0	3.44 7.9

Table 2: *Comparison of Experimental Average Separation in Muon Pairs vs MC Results for Different Rock Depth Intervals ($cos\theta = 0.8 \div 0.9$).*

Rock Depth (m w.e.)	R_0 $< D >$ exp. (m)	r.m.s. stat. R_0 $< D >$	Syst. err. $< D >$	MC Light R_0 $< D >$	MC Heavy R_0 $< D >$
$3350 \div 3750$	4.29 10.3	0.04 0.1	0.2	3.88 9.1	4.44 10.1
$3750 \div 4150$	3.91 9.7	0.05 0.1	0.3	3.37 8.1	3.82 8.9
$4150 \div 4550$	3.03 6.8	0.07 0.1	0.2	2.76 6.6	3.14 7.4
$4550 \div 4950$	2.63 6.6	0.07 0.2	0.3	2.44 6.1	2.86 6.9

MACRO supermodules shows that the average separation is greater than expected from the Monte Carlo. A detailed analysis of the possible systematic error due to the algorithms for the detector-independent analysis has shown that the maximum expected error on the average distance (10.9 m) is ± 0.2 m, not enough to reconcile data with simulation. We have also investigated the dependence of muon pair separation on rock depth and zenith angle. Tables 1 and 2 summarize the main results. It is worth noting that the experimental and simulated values follow the same behavior, and are close to one another. We observe again the same trend as for the overall distribution, that both the average distance between muons $< D >$ and the position of the maximum of the decoherence function R_0 are higher as measured by MACRO than as simulated.

Assuming that the heavy model is an extreme model, not confirmed by (or in disagreement with) the measurement of the muon flux, Fig. 5 may in-

dicate that the shower development is not yet treated properly in the Monte Carlo, and that the hadronic interaction model presently used for this analysis may need further improvement. In particular we are investigating factors which affect the transverse momentum distribution, including possible nuclear effects.

In order to better understand the role of the hadronic interaction model, we have performed a comparative simulation with the SIBYLL code [11]. No substantial changes, however, were observed as far as muon separation is concerned. Such a model in fact predicts a slightly lower average muon separation (on the order of 10% less). In the future other models will be considered, such as the DPMJET code [21], which has a more complete treatment of nuclear effects than does SIBYLL.

5 Muon Decorrelation

Detailed measurements of quantities relative to underground multiple muon events can provide information on primary interactions and muon propagation through the rock overburden. In particular, one can measure $\frac{dN}{dx\,d\phi}$, the differential distribution of spatial and angular separations in multiple muon events. This distribution is sensitive to the physics of muon production and in particular to the separation between primary interaction and muon detection; it is therefore also sensitive to the total primary cross section as well as to the transverse momentum distribution of the underground muons' parent hadrons. It also provides a measure of the effects of muon interactions in the rock overburden, which introduce displacements of the muons from their original direction and position. The aim of this analysis is to attempt to disentangle these effects.

The distribution can be derived analytically for a beam of muons at fixed energy and production height by treating multiple scattering in the rock in the gaussian approximation without fluctuations [22, 6]. The influence of primary interactions is contained in the lateral distribution of muons before they enter the rock:

$$Y(y) = Y(\frac{y}{\rho}) = \frac{dN}{dy} = \frac{E}{h_p}\,\frac{dN}{dp_t}. \qquad (6)$$

where $y = \frac{p_t}{E}\,h_p$ is the distance of the muon from the shower axis, h_p and

E are the production height and energy of the parent meson, $\rho = h_p \frac{p_t^0}{E}$ is the width of the distribution of distances from the shower axis, and p_t^0 is the width of the transverse momentum distribution.

The effect of propagation through the rock is contained in the distribution of muon displacements in angle θ and position r with respect to the original path of entry into the overburden:

$$G(r,\theta) = G(\frac{r}{\mu}, \frac{\theta}{\sigma}) \tag{7}$$

In real experiments there is little hope of reconstructing the entire distribution. What we have done is to measure the average relative angle as a function of the distance between muons in double muon events. We can distinguish three regimes in the behavior of the average angle $\langle\phi(x)\rangle$ (ϕ is the relative angle, and x the separation between pairs of muons in a bundle):

1. Small distances. Here the relevant contribution comes from small transverse momenta, and can generally written as:

$$\langle\phi(x)\rangle \sim \frac{\sqrt{3}}{2} \frac{\sigma\mu h_p^2 x}{\mu^2 h_p^2 + \rho^2(h_p + h_r)^2} \sim \frac{\sqrt{3}}{2} \frac{\sigma\mu x}{\mu^2 + \rho^2}; \tag{8}$$

   i. e. the average angular separation increases linearly with separation.

2. Moderate distances. Here, the result depends qualitatively on the *form* of the transverse momentum distribution at relatively large momenta. If the distribution decreases exponentially, then

$$\langle\phi(x)\rangle \sim \frac{\sqrt{3}}{2} \frac{\sigma\mu h_p}{\rho(h_r + h_p)} \sim (\text{constant}). \tag{9}$$

   If the decrease is slower, then $\langle\phi(x)\rangle$ tends to zero.

3. Large distances. For any transverse momentum distribution, the average angle increases linearly with separation:

$$\langle\phi(x)\rangle \sim \frac{x}{(h_r + h_p)}, \tag{10}$$

   where h_r is the distance traveled through the rock overburden.

A simple interpolating function valid at all distances is:

$$\langle\phi(x)\rangle = \frac{\sqrt{3}}{2}\frac{\sigma\mu x}{\mu^2+\rho^2+x\rho} + \frac{x}{h_p} \tag{11}$$

A priori, there is no reason why the relations derived in these approximations will be useful when the approximations are released. Their validity entirely depends upon how the parameters which determine the distribution fluctuate around their average values. We have compared these theoretical expectations with the distributions produced by a realistic, although simplified, simulation. In this simulation production height is fixed and an exponential transverse momentum distribution is used, but muon energies follow a realistic power law, and propagation through the rock overburden is treated realistically, including fluctuations. The results are presented in Fig. 6, together with the analytical results of Eq. 11. The agreement indicates that the analytical relations are at least a good guide for interpreting the experimental results.

In the analysis of these data we have so far used only double muon events and employed track reconstruction only in a projective view, namely the wire view. The results are still preliminary. Since the position of the shower axis is not known, the measure is relative; that is, the quantities ϕ and x are defined between pairs of muons in the same bundle. The distance is always taken to be positive, while the angle is positive if the tracks are diverging, and negative otherwise. Since the average angle as a function of distance is normalized to the number of events at that distance, the influence of apparatus effects (efficiency, working conditions, containment) should not be important. We have made no run selection on the data sample, but we have made an event selection rejecting too short tracks, to avoid contamination of the sample by locally produced pions and small showers. The experimental curve is presented in Fig. 7. We call this the "decorrelation" function since there is a linear correlation in the data at small distances that is less evident (if at all) at large distances.

In Fig. 7 we also plot the decorrelation function as computed from the HEMAS code. It is evident that there is a strong disagreement between the data and Monte Carlo at relatively small distances. From Eqs. 6 and 7 we see that the origin may be in the propagation (affecting σ and μ) or in the primary interaction (affecting ρ), and we have investigated several possible

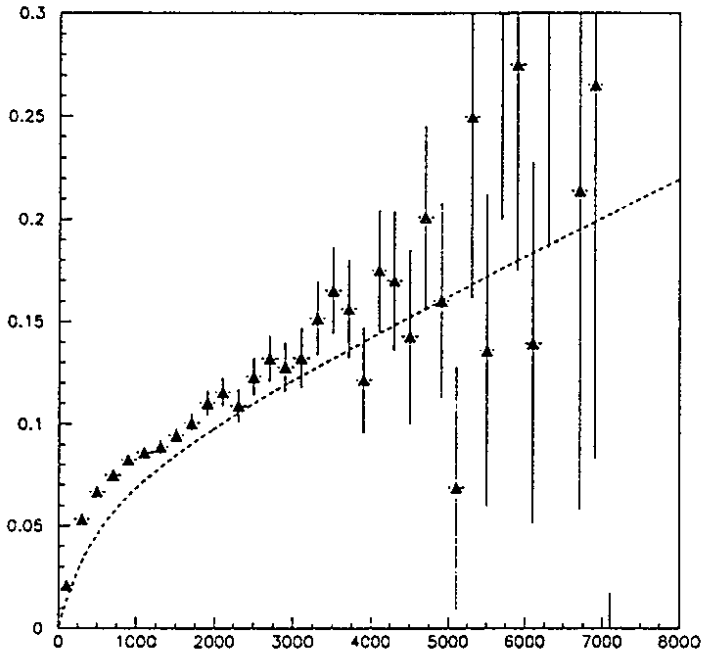

Figure 6: Average angle (deg) versus distance (cm). Data are from a simulation with $h_p = 30$ km and an exponential p_t distribution. The continuous line is the interpolation of Eq. 11 with parameters derived from the simulation.

causes. Different (extreme) composition models have essentially no effect. nor do more refined transport codes which include Molière tails beyond the Gaussian approximation. On the other hand, the modification of the average interaction cross section (and hence primary interaction height) needed to make the data and Monte Carlo agree is rather extreme, and likely inconsistent with reasonable extrapolations of accelerator data. We are presently investigating more subtle effects, both derived from the finite space resolution of the apparatus and from high energy interactions of muons in the rock overburden. Preliminary results are encouraging, but a more refined analysis is not yet complete.

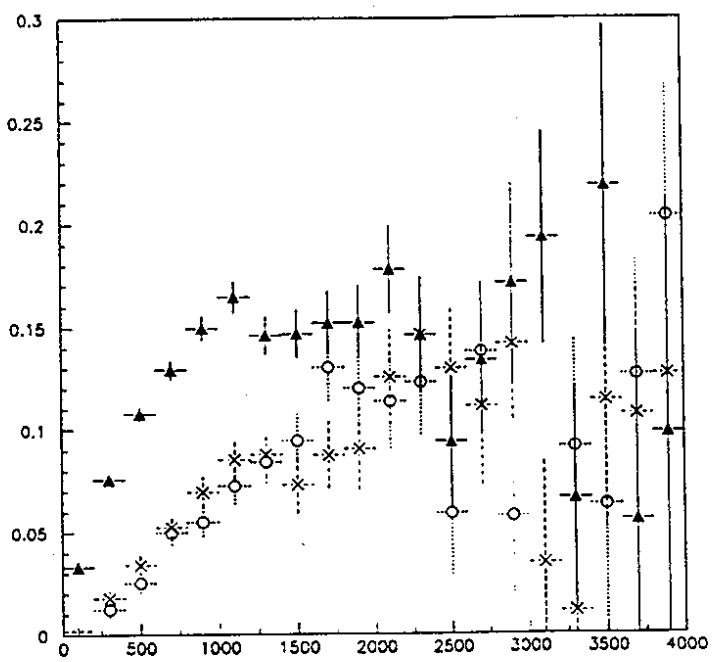

Figure 7: The decorrelation function as measured in MACRO (triangles) compared with the HEMAS predictions for the extreme light (crosses) and heavy (circles) composition models. Distances are in cm and angles in deg.

6 Delayed Muons

Searches for delayed particles in extensive air showers have been performed by several experiments [23, 24, 25, 26]. The presence of such particles in some searches was explained as rare signals of low energy hadrons [27] or as a decay product of heavy particles with long lifetimes [28]: Jones [29] pointed out that a quark with mass $m_q \simeq 10$ GeV and energy $E \simeq 100$ GeV produced 10 km above a given detector would arrive $\simeq 160$ ns behind the shower front. Relative delays of muons have been also been measured by Briatore *et al.* [30] at the Monte Cappuccini underground station (70 mwe), but these results were negative, placing an upper limit on such a free quark flux of $\varphi \leq 1.25 \times 10^{-11}$ cm^{-2}s^{-1}sr^{-1}. The muon bundles detected by MACRO can also be used to search for massive long lived particles, the main difference between our experiment and the others quoted above lying in the energy threshold of the detected particles, which is $E_\mu \geq 1.3$ TeV for our detector.

The present analysis concerns data obtained during the six month run using both the scintillator (SC) and streamer tube (ST) systems for the entire lower six MACRO supermodules. The main selection criteria were requiring the muon arrival time to be sampled with the central horizontal scintillator layer, considering only muon tracks reconstructed by the streamer tube system, and rejecting multiple muon hits in a single scintillator counter. A correction was applied for different muon path lengths. The total number of muon bundles selected is 51,236; they contain 109,039 muons.

We employed the variable $t_i^* = T^{bundle} - t_i$, where

$$T^{bundle} = \Sigma_{i=1}^{n_{bundle}} t_i / n_{bundle} \tag{12}$$

is the mean arrival time, t_i is the arrival time of the *ith* muon, and n_{bundle} is the detected bundle multiplicity. Fig. 8 shows the experimental t_i^* distribution, after path length correction, compared to a Monte Carlo simulation based both on the HEMAS code [9] and on real data. In order to obtain the relative time delay distribution t_i^{*h} for Monte Carlo muon events we simulated about twenty million showers using the HEMAS code and assuming the light model [20] for the primary cosmic ray composition.

Each muon in the real data set of multimuon events was treated as a stand alone track, and all muon tracks were required to hit both the central and the bottom planes of the MACRO scintillator system. For d equal to the path length between muon hits in the central and bottom scintillator layers, the t_i^{*}' distribution was computed by subtracting the quantity d/c from the bottom scintillator layer arrival time and comparing it to the central layer arrival time. The delays obtained in this manner are due to the scintillator system timing resolution. The final Monte Carlo t_i^* distribution is obtained by folding t_i^{*}' with the t_i^{*h} distribution (see Fig. 8). Note the good agreement between the data and the Monte Carlo prediction.

The simulation was repeated for different cosmic ray primary compositions. Fig. 9 shows the Monte Carlo distribution obtained using the light composition, a pure Fe composition with E=560 TeV/nucleus, and a pure Fe composition with E=5000 TeV/nucleus, respectively. Even in the case of these extreme compositions, the maximum spread of the time delay distribution is only $\simeq 200$ ps.

We conclude that the experimental t_i^* distribution is dominated by the scintillator timing resolution and that the experimental results are consistent

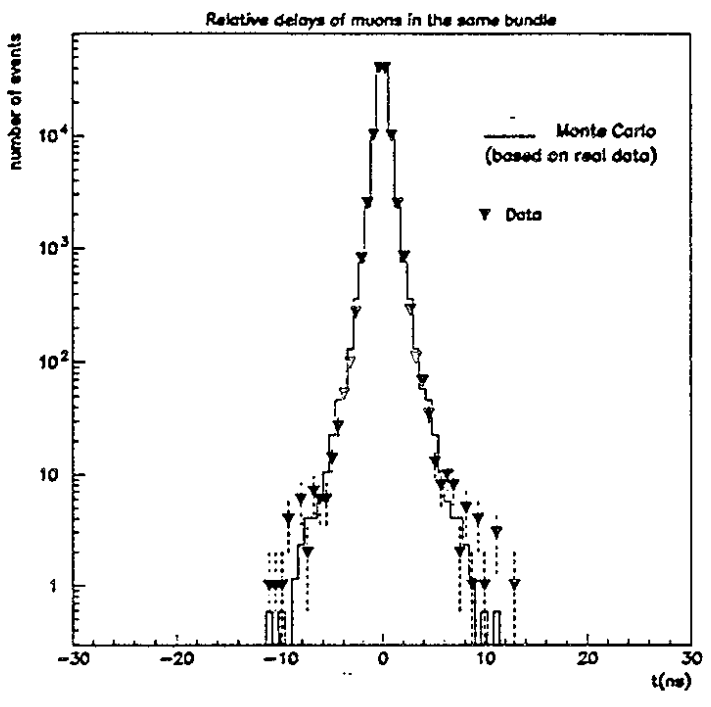

Figure 8: Muon delay distribution relative to the mean arrival time of the bundle. There is good agreement between the data and Monte Carlo (see text).

with standard physics, *i. e.* no massive particle is needed to explain our observations. Recently the CDF collaboration [31] at the Fermilab collider has placed an upper limit on the production cross section for long lived particles with mass in the range of 50 to 500 GeV, at the level of few tens of picobarns. In future analyses, we plan to include the production of massive stable penetrating particles in the HEMAS Monte Carlo. Using GMACRO, the MACRO detector simulation, we can estimate the detection efficiency for these exotic particles, and thus use experimental data to place an upper limit on their production cross section.

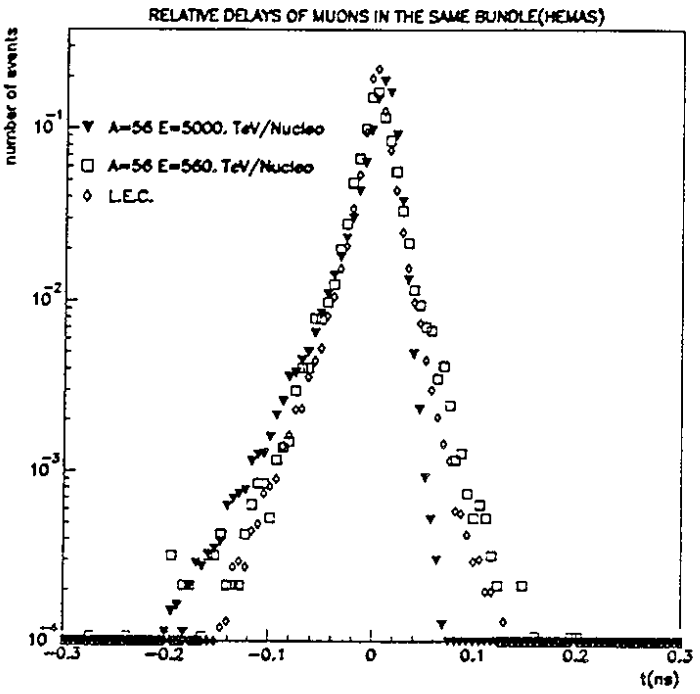

Figure 9: Muon delay distribution relative to the mean arrival time of the bundle. Even for extreme compositions the maximum spread is ~ 200 ps.

References

[1] The MACRO Collaboration (S. P. Ahlen *et al.*), *Phys. Lett. B* **249** 149 (1990).

[2] R. Brun *et al.*, CERN Publication DD/EE/84-1 (1992).

[3] H. Bilokon *et al.* LNGS Preprint 94/92 (1994).

[4] Ch. Berger *et al.*, *Phys. Rev. D* **40** 2163 (1989), and the EAS-TOP Collaboration (M. Aglietta *et al.*), *Nucl. Phys. B, Proc. Suppl.* **14** 193 (1990).

[5] T. K. Gaisser, *Cosmic Rays and Particle Physics*, Cambridge University Press: New York (1990).

[6] P. Lipari and T. Stanev, *Phys. Rev. D* **44** 3543 (1991).

[7] W. Lohman, R. Kopp, and R. Voss, CERN Publication EP/85-03 (1985).

[8] The MACRO Collaboration (S. P. Ahlen *et al.*), *Phys. Rev. D* **46** 895 (1992).

[9] C. Forti *et al., Phys. Rev. D* **42** 3668 (1990).

[10] J. Engel *et al., Proc. 22nd ICRC,* Dublin, **4** 1 (1991).

[11] R. S. Fletcher *et al.*, submitted to *Phys. Rev. D.*

[12] See for instance A. Capella *et al. Phys. Rev. Lett.* **58** 2015 (1987), and references therein.

[13] T. K. Gaisser and T. Stanev. *Phys. Lett. B* **219** 375 (1989).

[14] G. Auriemma *et al., Proc. 22nd ICRC,* Dublin, **2** 101 (1991).

[15] J. Kempa and J. Wdowczyk, *J. Phys. G* **9** 1271 (1983).

[16] The EAS-TOP and MACRO Collaborations (M. Aglietta, *et al.*), *Proc. 23rd ICRC.* Calgary, **2** 89 (1993).

[17] The MACRO Collaboration (S. P. Ahlen *et al.*), *Phys. Rev. D* **46** 4836 (1992).

[18] The MACRO Collaboration (S. P. Ahlen *et al.*), *Nucl. Instr. Meth. A* **324** 337 (1993).

[19] The MACRO Collaboration (S. P. Ahlen *et al.*). *Proc. 23rd ICRC,* Calgary, **2** 93 (1993).

[20] G. Auriemma *et al., Proc. 21st ICRC,* Adelaide, **9** 362 (1990).

[21] I. Kawrakov *et al., Phys. Rev. D* **47** 3849 (1993).

[22] A. F. Grillo and S. Parlati. LNGS Preprint 94/93, to be published in *Astroparticle Physics.* (1994).

[23] L. Jones *et al., Phys. Rev.* **164** 1584 (1967).

[24] S. C. Tonwar *et al., J. Phys. A* **5** 569 (1972).

[25] J. A. Goodman *et al., Phys. Rev. D* **19** 2572 (1979).

[26] P. N. Bath *et al., Phys. Rev. D* **25** 2820 (1982).

[27] A. Mineer *et al., Phys. Rev. Abs.* **16** 24 (1985).

[28] K. Watanabe and H. Sakuyama, MEISEI Report 83-4 (1983).

[29] L. Jones, *Rev. Mod. Phys.* **49** (1977).

[30] L. Briatore *et al., Proc. 14th ICRC* **7** 2405 (1975).

[31] F. Abe *et al., Phys. Rev. D* **46** R1889 (1992).